Appl Phys B (2011) 104:1035–1041
DOI 10.1007/s00340-011-4673-2

Applied Physics B
Lasers and Optics

Photon avalanche upconversion and pump power studies in $LaF_3:Er^{3+}/Yb^{3+}$ phosphor

A.K. Singh · K. Kumar · A.C. Pandey · O. Parkash · S.B. Rai · D. Kumar

Received: 10 August 2010 / Revised version: 4 June 2011 / Published online: 29 July 2011

Abstract Hexagonal $LaF_3:Er^{3+}/Yb^{3+}$ phosphor material has been synthesized by chemical precipitation method to obtain high near-infrared to green upconversion (UC) efficiency. Its thermal, structural and fluorescence properties have been studied. UC emission bands have been observed up to 315 nm in UV region. The effect of input pump power on the intensities of various emission bands has been studied in detail and photon avalanche UC mechanism has been identified. On increasing the excitation power, some bands have shown saturation in intensity. Also, at higher pump intensities two new UC bands were observed and their origin has been discussed. The phosphor has also been tested for possible UC-based fingerprint detection.

1 Introduction

Rare-earth (RE) doped upconversion (UC) materials received increased scientific interest because they are used in large number of applications, e.g. wavelength upconversion lasers, optical communication, optical temperature sensors, IR sensors, bioimaging, etc. [1–5]. Other potential applications of UC materials include light emitting devices, optical switches, fingerprint analysis, battlefield vehicle identification, solar cells, etc. [6–10]. New preparation routes and careful study of the upconversion materials could enhance the efficiency of existing materials and devices and could also reveal many new applications [11]. Among the upconversion phosphors, Er^{3+}/Yb^{3+} co-doped systems have shown the best upconversion efficiency and are, therefore, extensively used in these applications. Presently several highly efficient phosphor materials, viz. Er^{3+}/Yb^{3+} co-doped systems like $NaYF_4:Er^{3+}/Yb^{3+}$, $GdYF_4:Er^{3+}/Yb^{3+}$, $GdF_3:Er^{3+}/Yb^{3+}$, $LaF_3:Er^{3+}/Yb^{3+}$, $GdOS:Er^{3+}/Yb^{3+}$ (with UC efficiency as high as ∼26%) are available; however, efforts are still continuing to improve the luminescence performance of phosphors in the light of new advances in nanotechnology [12].

It is well known that phonon frequency of the host material decides the UC efficiency of the RE ion. Thus, there is a need to search for stable low phonon frequency host to attain high UC efficiency. LaF_3 works as a host efficiently (maximum phonon vibration frequency $<400\ cm^{-1}$) and is non-hygroscopic, whereas its oxides and sulfides are either hygroscopic or unstable. Crystal structure also plays a major role in achieving high UC emission. The best example of it is $NaYF_4:Er^{3+}/Yb^{3+}$[13]. Among the possible crystal phases, hexagonal phase has been found to be the best for achieving highest UC emission. Therefore, it is desirable to synthesize pure hexagonal-phase LaF_3 phosphor.

Er^{3+}/Yb^{3+} combination when pumped with cheaply available 976-nm diode laser gives number of UC emission bands with two most intense bands at 520–550 and 657 nm. It is highly desirable in some applications (fingerprint detection) to have UC emission only in green 520–550 nm region because human eyes are most sensitive to this wavelength region. Other emission bands degrade the emission efficiency of green wavelength. The intensity distribution

A.K. Singh · O. Parkash · D. Kumar (✉)
Department of Ceramic Engineering, IT, BHU, Varanasi 221005, India
e-mail: devendra.cer@itbhu.ac.in
Fax: +91-5422368428

K. Kumar · A.C. Pandey
Nanotechnology Application Center, Allahabad University, Allahabad 211002, India

S.B. Rai
Laser and Spectroscopy Lab., Physics Dept., BHU, Varanasi 221005, India

among the emission bands depends both on the ion concentration and on the properties of host matrix. So, either by tuning the concentration of RE or composition of host, one can achieve high green emission intensity. Objectives of the present work are: (1) to achieve high UC emission in hexagonal LaF_3:Er^{3+}/Yb^{3+} nanocrystalline phosphor using 976-nm excitation wavelength; (2) to get high intensity green emission; and (3) to check the possible fingerprint application of the present phosphor. The pump power dependence study has been carried out to understand the possible upconversion mechanism. Thermal and structural characterizations have also been carried out using different techniques.

2 Experimental

Chemical precipitation method was used for the synthesis of phosphor material. Reagent grade $La(NO_3)_3{\cdot}9H_2O$ (99.9%), $Er(NO_3)_3{\cdot}6H_2O$ (99.9%) and $Yb(NO_3)_3{\cdot}6H_2O$ (99.9%) were weighed in appropriate amount and dissolved in triply distilled water. After stirring about half an hour, drop-wise HF (46%) under stirring was added to the solution until pH of the solution became ∼4.0. The resulting white colloidal solution was boiled at 100°C for half an hour under stirring. After cooling down, the solution was filtered and white precipitate was collected. The precipitate was washed with water several times to remove the unused HF and then dried at 200°C for 24 hours. This as-synthesized powder sample was heat-treated (annealed) at 800°C and 1200°C for 2 hours under N_2 gas environment. Concentrations of RE ions were optimized for optimum UC emission. The UC emission was found optimal for 0.3 mol% Er and 2.0 mol% Yb concentration. Hence for further studies the sample with this concentration was used.

Differential thermal analysis (DTA) and thermogravimetric analysis (TGA) were carried out in a nitrogen gas atmosphere on a Perkin Elmer thermal analyzer in the temperature range 40–1200°C. The crystalline structure of the as-synthesized and heat-treated powder samples was determined by the powder X-ray diffraction (XRD) using Mo source. The obtained data were converted into Cu Kα pattern using software. Transmission electron micrographs (TEM) of the particles were taken using a Technai $30G^2$ (Philips) transmission electron microscope equipped with the charge-coupled device (CCD). Fourier transform infrared (FTIR) spectra of the samples were recorded using Spectrum RX-I spectrophotometer (Perkin Elmer). The luminescence spectra were recorded by exciting the sample with 976-nm radiation from a diode laser on an iHR320 spectrometer equipped with R928 photon counting photomultiplier tube.

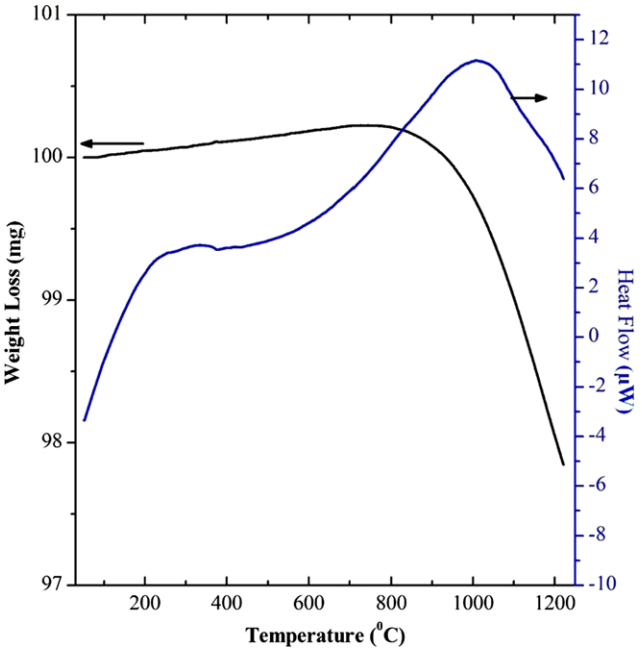

Fig. 1 Differential thermal analysis (DTA) and thermogravimetric analysis (TGA) curves of (0.3 mol%) Er^{3+} and (2.0 mol%) Yb^{3+} co–doped as-synthesized phosphor powder

3 Results and discussion

3.1 Thermal characterization

Figure 1 shows the DTA and TGA curves for as-synthesized sample. The DTA curve shows two exothermic peaks around 275°C and 1000°C. In the TGA graph, there is no weight loss at first DTA peak whereas second DTA peak around 1000°C is associated with a small weight loss of about 2%. This weight loss may be due to the removal of fluorine from the sample and exothermic nature of the peak is thought to occur from oxidation of the sample. From the DTA graph, it is clear that LaF_3 sample is stable up to 800°C.

3.2 Structural characterization

The as-synthesized and annealed samples at different temperatures for 2 hours were subjected to the XRD analysis. As-synthesized sample does not show any diffraction peak and is completely amorphous in nature. Figure 2 shows the XRD patterns of two batches of sample heat-treated at 800°C and 1200°C. From JCPDS data, single hexagonal-phase LaF_3 with space group $P\bar{3}c1$ has been found (JCPDS ID: 32-0483). The intensity of the XRD peaks decrease in the case of sample heat-treated at 1200°C. It is due to removal of F_2 from the sample which is also evident from the DTA analysis. The crystallite size t was estimated from the line broadening of XRD pattern using the Scherrer equation

$$t = \frac{\lambda \times 0.9}{\beta \times \cos\theta}$$

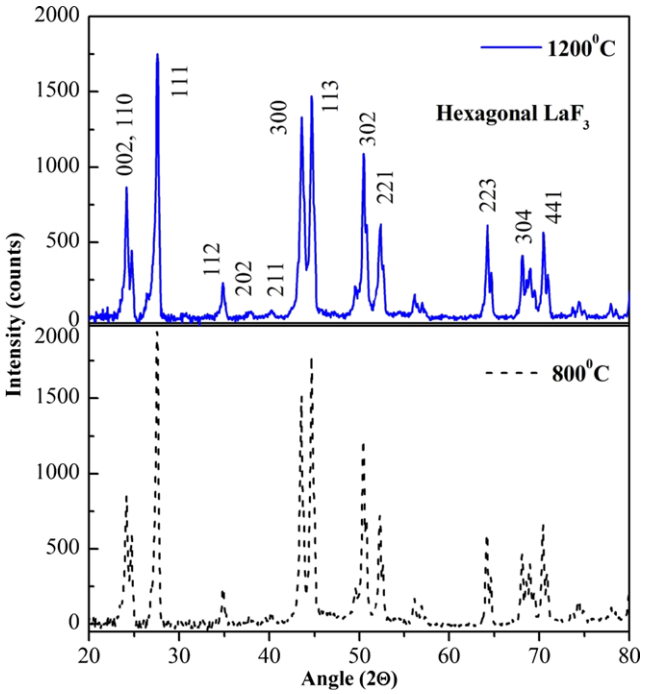

Fig. 2 X-ray diffraction pattern (XRD) of (0.3 mol%) Er^{3+} and (2.0 mol%) Yb^{3+} co-doped phosphor annealed at 800°C and 1200°C temperatures

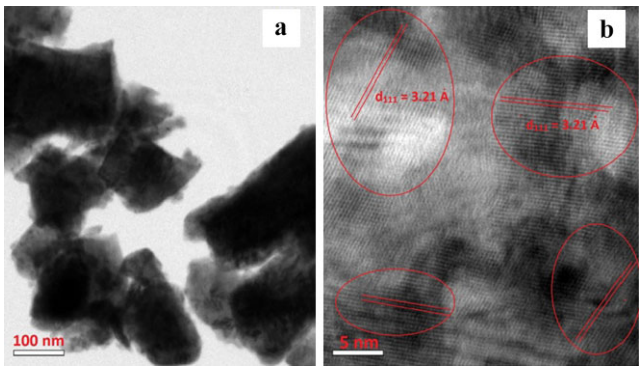

Fig. 3 Transmission electron micrograph of sample annealed at 1200°C; (**a**) at the 100 nm scale and (**b**) at the 5 nm scale

where λ is the wavelength of the incident X-ray radiation [CuK_α ($\lambda = 0.154056$ nm)], β is the full width at half-maximum (FWHM) in radians and θ is the diffraction angle for (h k l) plane.

Crystallite size calculation was carried out corresponding to the three most intense peaks. In case of sample annealed at 800°C the average crystallite size was 21–45 nm (in diameter) while for the sample annealed at 1200°C it was found to be around 19 ± 3 nm. This small decrease in crystallite size occurs due to the loss of fluorine from the sample that tends to decrease the grain boundaries in the samples. Figure 3 shows the TEM micrographs of sample annealed at 1200°C. From Fig. 3(a) it is evident that particle size is in the range of 200–300 nm which is much different from the size calculated by XRD analysis. The reason is that XRD calculation gives the crystallite size whereas TEM image visualizes particle size. A particle may have several crystallites. The high resolution TEM picture in Fig. 3(b) shows atomic planes with highly random orientation. It is concluded that there are lot of grain boundaries at nanometer level that separate crystallites from each other. The calculation from XRD analysis gives the size of these crystallites.

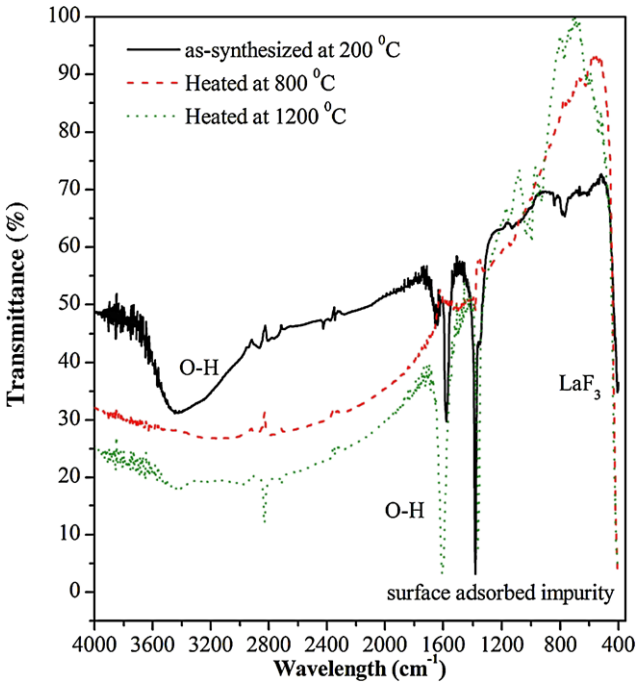

Fig. 4 FTIR spectra of as-synthesized and annealed samples

3.3 FTIR studies

Fourier transform infrared (FTIR) spectra of three samples viz. as-synthesized and annealed at 800°C and 1200°C are shown in Fig. 4. As-synthesized sample shows the presence of water as is evident from a broad absorption band at ~3412 cm^{-1} due to O–H stretching vibration. The characteristic IR peak located at 1600 cm^{-1} could be assigned to bending vibration of H_2O. As-synthesized sample also contains NO_3^- radical with its typical peak at 1386 cm^{-1}. NO_3^- radical comes from nitrate precursors. Sample annealed at 800°C does not show O–H vibration or any other impurities and is pure in its phase; however, sample annealed at 1200°C again shows the presence of water and CO_2 molecules. It appears that LaF (LaF_2) radical is very reactive and it easily absorbs water from atmosphere. Sample annealed at 1200°C is also thought to absorb some N_2 gas since a new vibration in this sample appears at 1366 cm^{-1}, which can be assigned

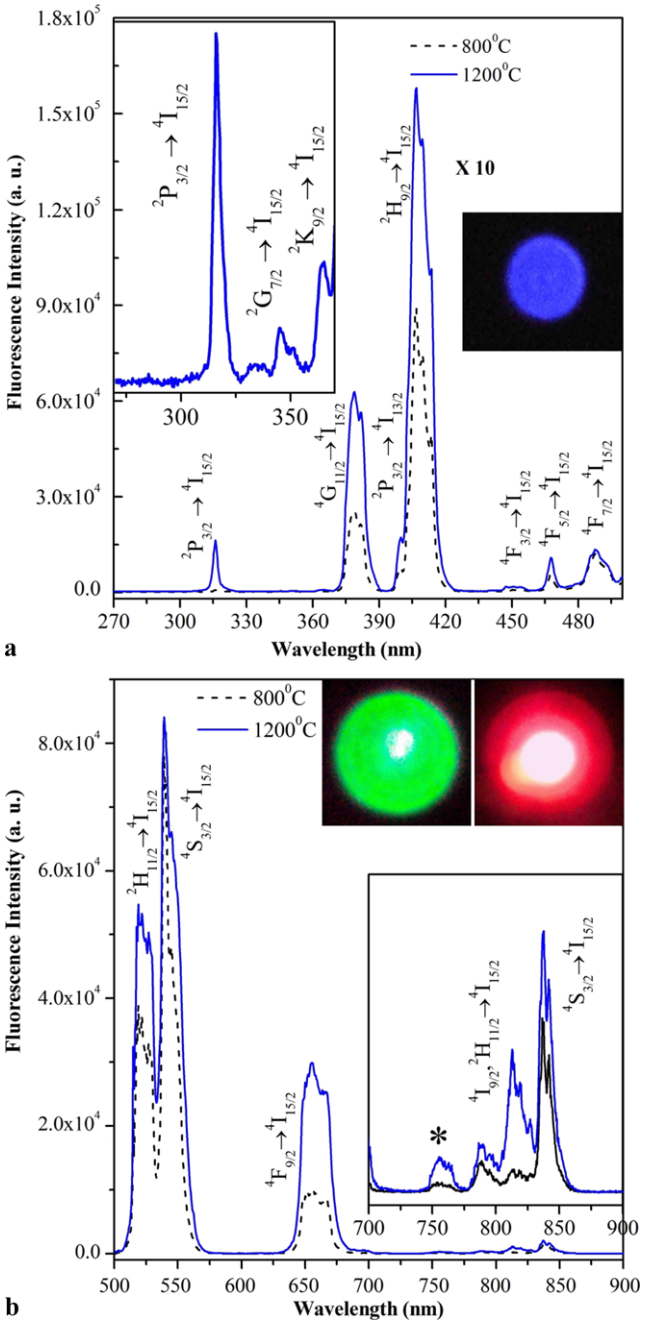

Fig. 5 (**a**) 976-nm excited upconversion emission spectra of 800°C and 1200°C annealed samples in the 270–500 nm region. An *inset on the left* shows the enlarged spectrum in UV region and *on the right* shows the photograph of blue emission. (**b**) 976-nm excited upconversion emission spectra of 800°C and 1200°C annealed samples in the 500–900 nm region. An *inset* shows the photograph of green and red emissions

to nitrogen bonded with other atoms of the phosphor. The highest energy La-F stretching vibration is expected below 400 cm^{-1}. FTIR spectra do not show vibrational mode of LaF_3 host.

3.4 Optical studies

3.5 Upconversion (UC) measurement

UC spectra of the samples on excitation with 976 nm are recorded in the 200–900 nm region. Figure 5 (a and b) shows the UC emission of the samples annealed at 800°C and 1200°C. Emission in case of as-synthesized sample is very weak and is not shown here. Intensity of emission increases with the increase in annealing temperature and a very intense emission is observed in case of both annealed samples. Intense red, blue and green colors could be easily seen with eyes using suitable filters. Inset of Fig. 5 (a and b) shows digital photograph of the fluorescence emission in blue, green and red regions for sample annealed at 1200°C. UC emission bands with wavelengths as small as 316 nm could be observed in the present case. Intense bands are observed at 378, 407, 521, 540 and 657 nm. The transitions of the bands are assigned in the Fig. 5 (a and b). The UC band at 316 nm is rarely reported in Er^{3+}/Yb^{3+} system since the emission yield towards the UV region successively decreases and it becomes hard to detect emission. In LaF_3:Er^{3+}/Yb^{3+} this emission is intense enough and is much higher than its oxide La_2O_3:Er^{3+}/Yb^{3+} sample [14]. La_2O_3:Er^{3+}/Yb^{3+} sample, on the other hand, shows emission in deep UV region at 235 nm due to the $^2I_{11/2} \rightarrow {}^4I_{15/2}$ transition which is not observed in the case of LaF_3 sample.

Annealing of the sample above 1000°C degrades the quality of the sample due to removal of F_2 from the sample. Sample annealed at 1200°C shows better enhancement in UV emission (Fig. 5); however, green emission intensity remains almost the same. It was noted that sample loses some fluorine at 1200°C and thus becomes weakly hygroscopic in nature. Sample left in open atmosphere for prolonged time shows decrease in overall emission intensity. Red emission (657 nm) for this sample is found more enhanced than for the sample annealed at lower temperature. This effect of annealing on the emission enhancement can be interpreted on the basis of DTA and XRD analysis. Both DTA and XRD show decrease in fluorine content in the sample annealed at 1200°C. Due to this fluorine reduction, defects in the sample form that enhance electron–phonon interaction strength. This increase in interaction enhances non-radiative relaxation from $^4S_{3/2}$ level to $^4F_{9/2}$ level and due to this, population in $^4F_{9/2}$ level (red emission) increases. The following reaction may take place:

$$LaF_3 \xrightarrow{1200^\circ C} (LaF_3)_{\text{F defficient}} + F_2 \uparrow + V_F^{\bullet}$$

From the emission spectrum, it is clear that most part of the total integrated UC emission intensity falls in the green 520–540 nm region. When it is compared with La_2O_3:Er^{3+}/Yb^{3+} phosphor, a better green emission with

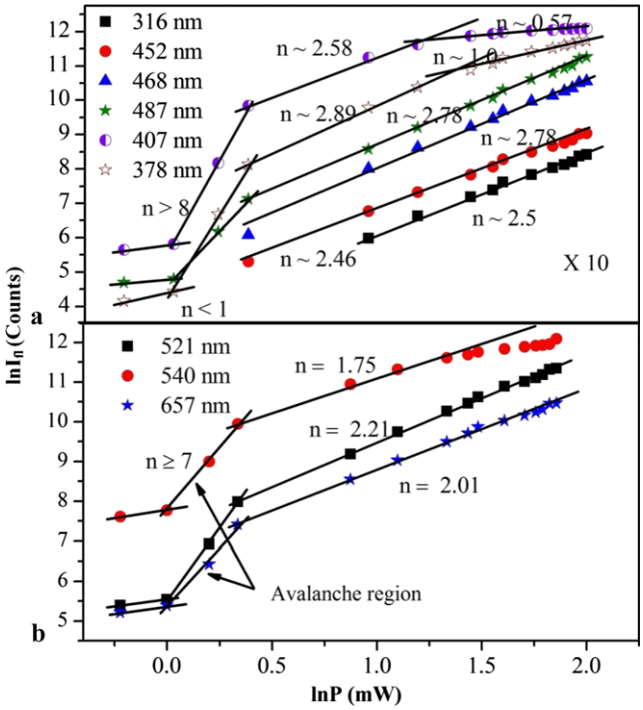

Fig. 6 $\ln(I_{fl})$–$\ln(P)$ plots (fluorescence intensity versus power) for various bands; the number denotes the photons involved in that particular transition. (**a**) For 200–500 nm, and (**b**) for 500–900 nm band region

double intensity is observed in fluoride. Inset of Fig. 5(b) compares the UC emission intensity between the two phosphors in the 500–700 nm region. Human eyes are most sensitive to green radiation, so it is desirable to have phosphor that emits only in the green region. In the present study, LaF_3 host has been found better than its oxide host.

Yi and Chow [15] in their studies have found that UC efficiency of $LaF_3:Er^{3+}/Yb^{3+}$ is several times greater than the well-known $NaYF_4:Er^{3+}/Yb^{3+}$ phosphor which has about 24% UC efficiency. The authors relate the increased UC efficiency in LaF_3 host due to its hexagonal phase whereas the latter has a cubic symmetry. Though, hexagonal $NaYF_4:Er^{3+}/Yb^{3+}$ phosphor has also been reported in the literature. Along with the host geometry, the phonon frequency of host matrix plays a major role in UC efficiency. $NaYF_4$ lattice has its maximum phonon frequency $\sim$418 cm^{-1}, whereas LaF_3 has its maximum phonon frequency $<$400 cm^{-1}. These two factors make $LaF_3:Er^{3+}/Yb^{3+}$ highly UC-efficient phosphor.

3.6 Power dependence and lifetime studies

In order to understand the UC mechanisms involved in emissions, the emission intensities (I) of various bands were recorded as function of laser pump power (P). Intensity of the emission follows $I_{\text{emission}} \propto P^n_{\text{pump}}$ rule, where n decides the number of incident photons involved in the emission of upconverted photons. The pump power dependence plots for various bands are shown in Fig. 6. Bands show varying slopes with the increase in power. Some bands also show saturation behavior. From Fig. 6 four regions in the plots are obvious:

1. Region 1: This is the region where slope is less than expected. As an example, for the emission at 378-nm wavelength, the least number of required input photons is $n = 976/378 = 3$ but from graph it comes around 1;
2. Region 2: This is the region where slope is much more than expected. The highest energy band is observed at 315 nm which will involve 3 or 4 IR photons to reach $^2P_{3/2}$ level as in our previous work [14]. But in this case, all the plots show slope >8 in this region;
3. Region 3: It is the region where slopes are near the expected value;
4. Region 4: It is the saturation region where populations in the excited levels get saturated.

A further increase in the excitation power results in decrease in emission intensity.

The different regions in the pump power plots occur due to the competition between various energy transfer mechanisms and also between radiative and non-radiative channels. In the present case, three excitation mechanisms—excited state absorption (ESA), photon avalanche (PA) and energy transfer (ET)—play role in upconversion emission. Competition among these mechanisms results in different slopes of the various emission bands.

The model proposed by Pollnau et al. [16] is sufficient to explain the behavior in regions 3 and 4 but inadequate to explain that in regions 1 and 2. To explain region 1, it can be taken that mechanism for regions 1 and 4 is the same. In region 1, non-radiative rate dominates over the radiative process. Also, radiative process mainly occurs through down-conversion emission and only a small part of the input radiation converts into UC emission. Both the non-radiative and down-conversion emissions result in low slope values for UC bands. As the pump power increases and reaches above certain threshold value, a sudden increase in the slope value is observed (region 2). This is the photon avalanche region. The mechanism of photon avalanche has been explained for many RE phosphors. In the present case only bands at 407 and 378 nm show region 4 and other bands do not show saturation at higher powers.

Bands at 451 and 467 nm due to $^4F_{3/2} \rightarrow {}^4I_{15/2}$ and $^4F_{5/2} \rightarrow {}^4I_{15/2}$ transitions appear relatively at higher pump powers. These bands do not show saturation in pump power behavior. It is interesting to consider the mechanism for these emissions. Here it appears that local thermalization of the $^4F_{3/2}$ and $^4F_{5/2}$ levels with $^4S_{3/2}$ level occur at higher pump power. The non-radiative processes result in an increase of the temperature of the sample at the point of ir-

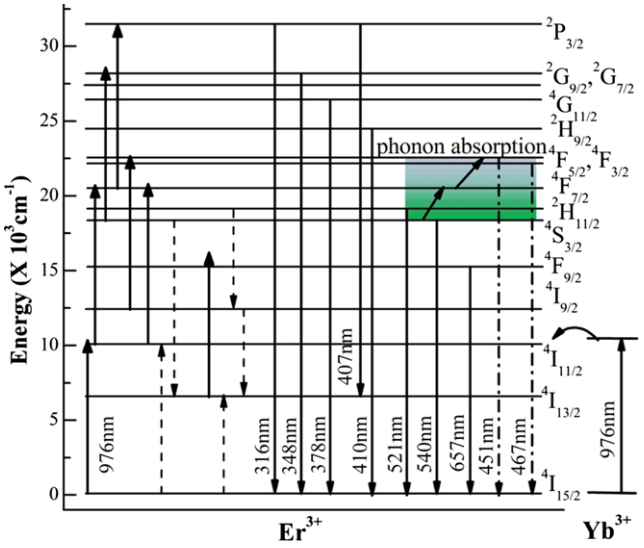

Fig. 7 Schematic representation of emission pathways for different emission bands

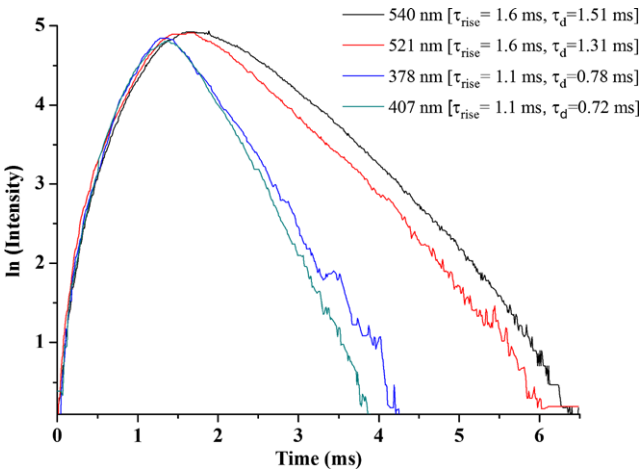

Fig. 8 Decay patterns of various emission bands with 976-nm excitation

radiation. The increased samples' temperature causes thermalization between the above said levels. In Fig. 7, various mechanisms involved in different emission bands are schematically represented.

Lifetime of UC emission bands for sample annealed at 1200°C has been recorded using the same excitation. Decay curves of four emitting levels are shown in Fig. 8. The level $^4S_{3/2}$ gives lifetime of 1.51 ms whereas the level $^2H_{11/2}$ shows a lifetime of 1.31 ms. The lifetime of $^2H_{11/2}$ level should be low according to the theory but this large lifetime occurs due to thermalization of this level with $^4S_{3/2}$ level. Both the levels show rise time around 1.66 ms. Levels $^4G_{11/2}$ and $^2H_{9/2}$ show lifetimes 0.78 and 0.72 ms, respectively, and both have equal rise time (∼1.1 ms). The significance of equal rise time is that both the levels are populated

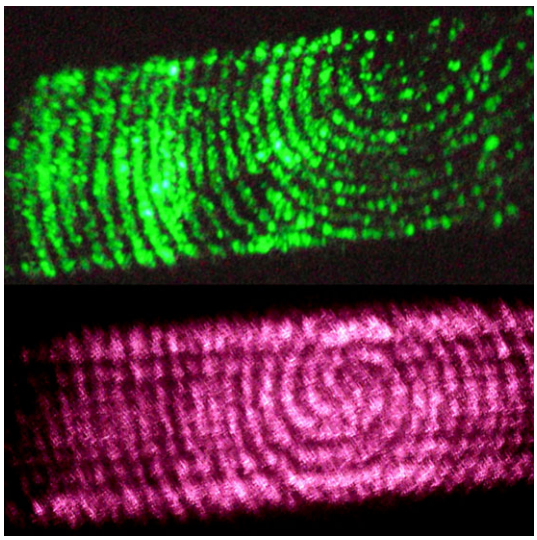

Fig. 9 Fingerprint developed in green and red colors using Er^{3+}/Yb^{3+} co-doped LaF_3 powder illuminated by a 976-nm diode laser at 300-mW power

through the same excitation procedure through the same intermediate state.

3.7 Application to fingerprinting

The excellent UC emission property of the powder phosphor can efficiently be used to identify the latent fingermarks on hard surfaces where conventional technique has its limitation. The synthesized phosphor has been checked for possible use of it in latent fingerprint identification in multicolored mode on hard colored surfaces. The phosphor nanopowder was sprinkled on the fingermarks made on glass plate using the conventional powder dusting technique [17] and then illuminated by a 976-nm diode laser emitting 300 mW power. The images were simply photographed by a Kodak Easyshare CX6330, 3.1 megapixel camera. Fingerprints developed in two different colors (red and green) on the glass are shown in Fig. 9. A clear contrast between the fingerprint ridges and the background is visible. Also, the present phosphor shows a better visibility than our previously used phosphor for the same purpose [14] because of the improved UC emission in LaF_3:Er^{3+}/Yb^{3+}. It is estimated that full area fingermarks can be observed using a 2-W circular beam diode laser in place of 300-mW currently used laser.

4 Conclusions

High IR to green upconversion efficient stable fluoride phosphor material doped with Er^{3+}/Yb^{3+} has been synthesized and its upconversion properties have been studied. Pump power study has shown that the material undergoes different

upconversion mechanisms with increasing pump power and avalanche mechanism in the intermediate region. The lifetimes of green and blue emitting levels have been recorded. The material has been checked for possible latent fingerprint recording and has shown good prospect for this application.

References

1. F. Azuel, Chem. Rev. **104**, 139 (2004)
2. W.M. Yen, S. Shionoya, H. Yamamoto, *Practical Applications of Phosphors* (CRC Press/Taylor & Francis, Boca Raton, 2006)
3. A. Rapaport, J. Milliez, M. Bass, A. Cassanho, H. Jenssen, J. Disp. Technol. **2**, 68 (2006)
4. http://www.phosphor-technology.com/index.htm
5. H.A. Hoppe, Angew. Chem. **48**, 3572 (2009)
6. V.K. Tikhomirov, L.F. Chibotaru, D. Saurel, P. Gredin, M. Mortier, V.V. Moshchalkov, Nano Lett. **9**, 721 (2009)
7. S.K. Singh, K. Kumar, S.B. Rai, Appl. Phys. B **94**, 165 (2009)
8. I.-F. Shih, D.B. Chang, US Patent, 2005, No. US 6849855 B1
9. A. Shalav, B.S. Richards, T. Trupke, K.W. Krämer, H.U. Güdel, Appl. Phys. Lett. **86**, 013505 (2005)
10. K. Binnemans, Chem. Rev. **109**, 4283 (2009)
11. V.K. Tikhomirov, K. Driesen, V.D. Rodriguez, P. Gredin, M. Mortierand, V.V. Moshchalkov, Opt. Express **17**, 11794 (2009)
12. F. Wang, X. Liu, Chem. Soc. Rev. **38**, 976 (2009)
13. J.F. Suyver, J. Grimm, M.K. van Veen, D. Biner, K.W. Kramer, H.U. Gudel, J. Lumin. **117**, 1 (2006)
14. S.K. Singh, A.K. Singh, D. Kumar, O. Prakash, S.B. Rai, Appl. Phys. B, Lasers Opt. **98**, 173 (2010)
15. G.-S. Yi, G.-M. Chow, J. Mater. Chem. **15**, 4460 (2005)
16. M. Pollnau, D.R. Gamelin, S.R. Lüthi, H.U. Güdel, M.P. Hehlen, Phys. Rev. B **61**, 3337 (2000)
17. C. Champod, C. Lennard, P. Margot, M. Stoilovic, *Fingerprint and Other Ridge Skin Impression* (CRC Press, Boca Raton, 2004)